

Gareth J Berry<sup>1</sup>, Chris Thorncroft<sup>1</sup> and Tim Hewson<sup>2</sup>.

<sup>1</sup>University at Albany/SUNY, Albany, New York, USA.

<sup>2</sup>Met Office, Exeter, UK.

## 1. INTRODUCTION.

Discussion and interpretation of easterly wave (EW) developments ideally requires a consistent reference point to be identified. Historically this has been quite challenging because the multiple scales involved are difficult to disentangle. Previous studies (e.g. Reed et al, 1977) have tended to use mid tropospheric trough and ridge axes, generally defined by a change in sign of the meridional wind field (i.e.  $v = 0 \text{ m s}^{-1}$ ), as the reference point (and implicitly as the definition) for an EW. However, this diagnostic is not Galilean invariant and the distinction between EWs and other phenomena of overlapping scale (such as a large mesoscale convective complex (MCC)) is not always obvious. This could result in unrelated phenomena being identified as EWs.

In this research we propose a new objective method of identifying EWs. Following the methodology used by Hewson (1998) to objectively identify mid-latitude fronts, we present a simple, accurate and customizable way of identifying and plotting EWs that can be applied to any gridded dataset. We then use this technique to document African Easterly Waves (AEWs) that during July, August and September (JAS) in both 2004 and 2005. We focus on AEW activity over the African continent for comparison with composite structures and conceptual models.

## 2. DESCRIPTION OF THE DIAGNOSTICS.

It is desirable at the outset to define both a unique characteristic and a consistent reference point for the synoptic examination of AEWs. It is also highly advantageous for forecasting purposes to have a diagnostic that is easy to interpret and can be generated in real time with minimal computation from standard observed or modeled fields. Because of its familiar nature and deployment in previous studies, the core diagnostic chosen in this research is the position of the AEW trough axis.

We suggest that AEW trough axes should be ideally defined based on streamfunction ( $\psi$ ). Streamfunction has the distinct advantage that the

elimination of the divergent flow reduces noise associated with individual MCCs and offers a smoother field that presents less technical difficulties for the computation of objective AEW trough axes. Maximum perturbations associated with AEWs have been observed to occur near the level of the African Easterly Jet (AEJ, e.g. Reed et al, 1977), i.e. near 650hPa. We define AEW trough axes on the basis of  $\psi$  at 700hPa, as this is the closest standard atmospheric level.

For orientation, an example of the 700hPa  $\psi$  field over tropical North Africa during September 2004, as computed from output from a global model, is shown in Fig.1. Recalling that the zonal ( $u_\psi$ ) and meridional ( $v_\psi$ ) components of the non-divergent wind ( $\vec{V}_\psi$ ) are given by:

$$u_\psi = -\frac{\partial \psi}{\partial y} \quad (1) \quad \text{and} \quad v_\psi = \frac{\partial \psi}{\partial x} \quad (2),$$

reveals that the non-divergent wind in the tropics is essentially the counterpart of the geostrophic wind in the extratropics. Figure 1 shows a large-scale anticyclone between 20 and 30°N, west of the Greenwich meridian, marking the upper portion of the Saharan heat low circulation. On the equatorward flank of this mid-level anticyclone (between 10 and 20°N) a zonally elongated band of enhanced  $\psi$  gradient can be observed, denoting the approximate location of the AEJ. The signature of an AEW is a wavelike perturbation to this intense gradient that moves westwards with time. The position of a trough axis is marked by a poleward displacement of the  $\psi$  contours and a ridge by an equatorward displacement. Two prominent troughs can be seen in Fig.1 (labelled 'T'). The streamfunction field can in fact be used, in isolation, to compute diagnostic quantities that enable AEWs, and indeed the AEJ, to be plotted objectively (in line segment format).

Using the non-divergent wind components, we compute 'streamfunction vorticity' ( $\xi_\psi$ ) defined as

$$\xi_\psi = \nabla_h \times \vec{V}_\psi \quad (3).$$

Where  $\nabla_h$  is a standard horizontal gradient operator and the computed streamfunction vorticity is implicitly a vertical component. This quantity is displayed in Fig.2 (positive values only), superimposed on the source  $\psi$  field, which has been shown in Fig.1.

---

Corresponding Author Address:

Gareth J Berry, ES-333, Department of Earth and Atmospheric Sciences, University at Albany, SUNY, 1400 Washington Ave, Albany, NY 12222. Email: gareth@atmos.albany.edu

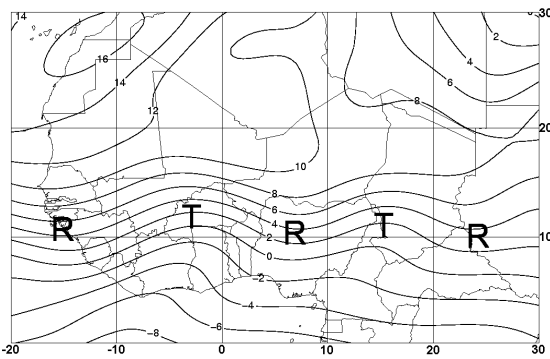


**Figure 1** - Example of the 700hPa streamfunction ( $\psi$ ) field over North Africa. Values are contoured every  $2 \times 10^6 \text{ m}^2 \text{ s}^{-1}$ . Labels 'T' and 'R' indicate the axes of trough and ridge respectively.

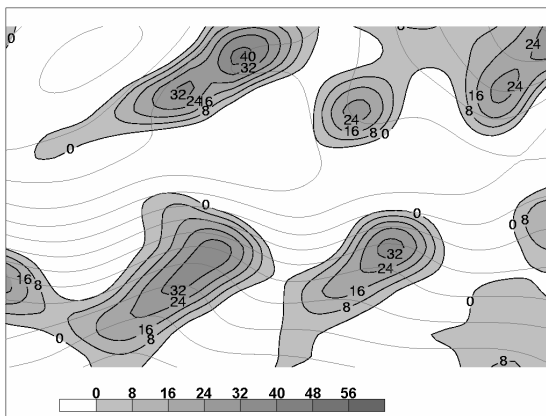


**Figure 2** - Streamfunction vorticity of the source  $\psi$  field shown in Fig. 1. (positive values only shaded according to scale, units of  $10^6 \text{ s}^{-1}$ )

From the streamfunction vorticity the position of a trough or ridge can be simply defined as:

$$-\vec{\nabla}_\psi \bullet \nabla_h \xi_\psi = 0 \quad (4)$$

i.e. the point where the advection of the streamfunction vorticity by the non-divergent wind is equal to zero. This concurs with synoptic reasoning – wherein positive vorticity advection lies ahead of a trough axis and negative vorticity advection behind. However, this definition of trough and ridge lines is only mathematically correct for idealized 2-dimensional waves (i.e. where  $\vec{\nabla}_\psi$  is a function of only one horizontal direction). Those that occur over tropical North Africa are not of this type. This is because a large contribution to the total streamfunction vorticity comes from horizontal shear across the AEJ. The advection of streamfunction vorticity due to the westward propagation of AEWs is obscured by the advection associated with relatively small fluctuations in the position or nature of the AEJ. A simple solution is achieved by partitioning the streamfunction vorticity into that due to the shear of the non-divergent wind

(referred to here as 'streamfunction shear vorticity') and that due to the curvature of the non-divergent wind field (henceforth referred to as 'streamfunction curvature vorticity'), i.e.

$$\xi_\psi = \xi_\psi^{\text{Shear}} + \xi_\psi^{\text{Curvature}} \quad (5).$$

Note again that each term in (5) is implicitly a vertical component, computed solely from the horizontal non-divergent wind field. The two components of streamfunction vorticity, for the source  $\psi$  field, are shown in Fig.3 (positive values only).

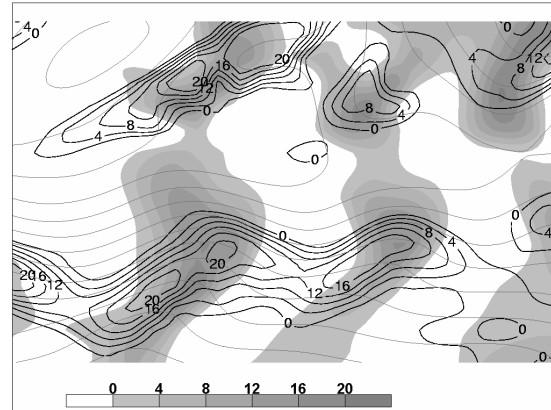


**Figure 3** - Streamfunction vorticity of the source  $\psi$  field shown in Fig. 1, split into curvature (positive values shaded according to scale, units of  $10^6 \text{ s}^{-1}$ ) and shear (dark contours drawn every  $4 \times 10^6 \text{ s}^{-1}$  above zero)

The AEW trough and ridge axes are then re-defined to be where:

$$-\vec{\nabla}_\psi \bullet \nabla_h \xi_\psi^{\text{Curvature}} = 0 \quad (6).$$

This contour is shown on the source  $\psi$  field in Fig.4:



**Figure 4** - Contours where the advection of streamfunction curvature vorticity by the non-divergent wind is equal to zero (equation (6), thick black lines) on top of source  $\psi$  field (grey contours).

In order to differentiate between AEW troughs and ridges, masks must be used to eliminate unwanted lines (i.e. for our purposes AEW ridges), one mask is applied to obscure lines wherever the streamfunction curvature vorticity is below a (positive) threshold value, resulting in only trough lines being displayed. Because there will be instances where the curvature of the non-divergent wind field reaches a local minimum, yet is still positive (or conversely reaches a local maximum, yet is still negative) a further masking diagnostic is required, to remove spurious lines that are not removed by the streamfunction curvature vorticity mask:

$$\vec{V}_\psi \bullet \nabla_h (-\vec{V}_\psi \bullet \nabla_h \xi_\psi^{Curvature}) > K \quad (7)$$

where  $K$  is greater than or equal to zero for plotting troughs (for ridges the inequality sign would be reversed and  $K$  would be less than or equal to zero). This mask operates by determining whether the gradient of the advection of streamfunction curvature vorticity has a component in the direction of non-divergent wind; for troughs positive advection occurs ahead (downstream) of the trough, making the left hand side of (7) positive.

Note that lines along which streamfunction shear vorticity ( $\xi_\psi^{Shear}$ ) equals zero denote the cores of non-divergent wind speed maxima or minima<sup>3</sup>. Jet cores (i.e. wind speed maxima) are isolated by using the following graphical mask:

$$\vec{V}_\psi \bullet ((\nabla_h \xi_\psi^{Shear}) \times \hat{k}) > 0 \quad (8)$$

where  $\hat{k}$  is the unit vector perpendicular to the Earth's surface (and the  $\times \hat{k}$  operator effects a 90 degree clockwise rotation of the preceding vector). Effectively this mask detects whether streamfunction shear vorticity is positive to the left or right of the non-divergent wind vector. If it is positive to the left the extrema must be a maximum, the inequality will be positive and the jet axis will be retained. If it is positive to the right the extremum must be a minimum, the inequality will be negative and the (anti-) jet will be erased.

Figure 5 shows Fig.4 after the application of the aforementioned graphical masks (i.e. curvature vorticity threshold, equations (7) and (8)). This procedure isolates the AEW trough axes (shown as thick black contours) and the AEJ core (shown as dashed black contour). Note in this instance we have also obscured trough lines in regions where  $u_\psi$  is greater than  $0\text{ms}^{-1}$ , since we are interested in synoptic systems embedded in easterly flow.



**Figure 5** – As in Fig.4, except with the addition of masks that exclude equation (6) in regions of streamfunction curvature vorticity below  $0.5 \times 10^{-5}\text{s}^{-1}$ , where there is westerly flow and where equation (7) does not hold for  $K=0\text{ ms}^{-1}$ . This isolates the AEW trough axes (thick black lines). Also shown is the shear vorticity equal to zero contour, representing the AEJ core (dashed black line), in regions where equation (8) holds and where the magnitude of the non-divergent wind is greater than  $8\text{ms}^{-1}$ .

### 3. APPLICATION OF THE DIAGNOSTICS.

The diagnostics described in the previous section were generated for July, August and September 2004 and 2005 using  $1^\circ \times 1^\circ$  National Centers for Environmental Prediction (NCEP) Global Forecast System (GFS) operational analyses (which have a temporal resolution of 12 hours).

Long-lived synoptic scale trough axes were tracked manually over the African continent and Atlantic Ocean, utilizing the intersection of the trough and jet axes as an objective reference point in each case (see Berry et al (2006) for detailed information of the tracking criteria). Basic statistics were compiled (including origins and fates of the systems) and detailed synoptic analyses were conducted.

### 4. RESULTS.

The major results from this manual tracking, with detailed discussion are documented in Berry et al (2006). Table 1 below shows the total number of AEWs based on the diagnostics that were generated over the African continent during July, August and September 2004 and 2005.

	Jul	Aug	Sep	Total
2004	11	12	8	31
2005	8	9	8	25

**Table 1** – Number of AEWs identified using the objective technique during 2004 and 2005.

It is evident from table 1 that the number of AEWs during both years is close to that expected based on the periodicity of AEWs found in previous studies (e.g. Burpee, 1974). It was noted that the 'Average' AEW observed during both seasons bore distinct similarity to those observed in composite

<sup>3</sup> This was essentially the method used to identify and plot jet stream cores on two of the figures in Hewson (1998) (albeit with shear vorticity used rather than streamfunction shear vorticity).

studies (e.g. Reed et al, 1977). However, it was also noted that each AEW possessed unique qualities that require more detailed investigation. An Example of this pronounced case-to-case variability is obtained from the mean speed and initial location of AEWs during 2004, which varied between  $5\text{--}15\text{ ms}^{-1}$  and  $11^\circ\text{W}\text{--}34^\circ\text{E}$ , with standard deviations of  $2.8\text{ ms}^{-1}$  and  $11.8^\circ$  respectively.

From the synthesis of the synoptic analyses it was observed that mature AEWs structures over the African continent varied, ranging from isolated potential vorticity maxima confined equatorward of the objectively-defined AEJ, to broad cross-jet structures symptomatic of both baroclinic and barotropic growth. As many as 80% of the cases during 2004 fell into the second category. Figure 6 is a sequence of images showing an example of this second category of AEW structure. After leaving the West African coast, 45% of the AEWs tracked in 2004 were associated with tropical cyclogenesis in either the Atlantic or Pacific Ocean basins.

## 5. OUTLOOK.

Future work will be focused on both the expansion of the objective diagnostics (e.g. by coupling with an automated track algorithm) and application in different circumstances (e.g. for the examination of equatorial Kelvin waves in filtered data). In its present form, the diagnostics can be used as a simple model verification tool (e.g. by generating 'spaghetti plots'). Such products could be used to gauge confidence at a particular forecast time or even to examine model biases. During the summer months (resource allowing) a website will be generating these diagnostics for tropical North Africa and the tropical Atlantic Ocean in near real-time using the GFS analysis and forecast products. This can be found at: <http://www.atmos.albany.edu/student/gareth/plots.html>

## 6. REFERENCES.

Berry, G. J. and C. Thorncroft and T. Hewson, 2006: African Easterly Waves during 2004: Analysis using objective techniques. *Mon. Wea. Rev.* Accepted.

Burpee, R. W., 1974: Characteristics of North African easterly waves during the summers of 1968 and 1969. *J. Atmos. Sci.*, **31**, 1556–1570.

Hewson, T.D. 1998: Objective fronts. *Meteorol. Appl.*, **5**, 37–65

Reed, R. J., D. C. Norquist, and E. E. Recker, 1977: The structure and properties of African wave disturbances as observed during phase III of GATE. *Mon. Wea. Rev.*, **105**, 17–33.

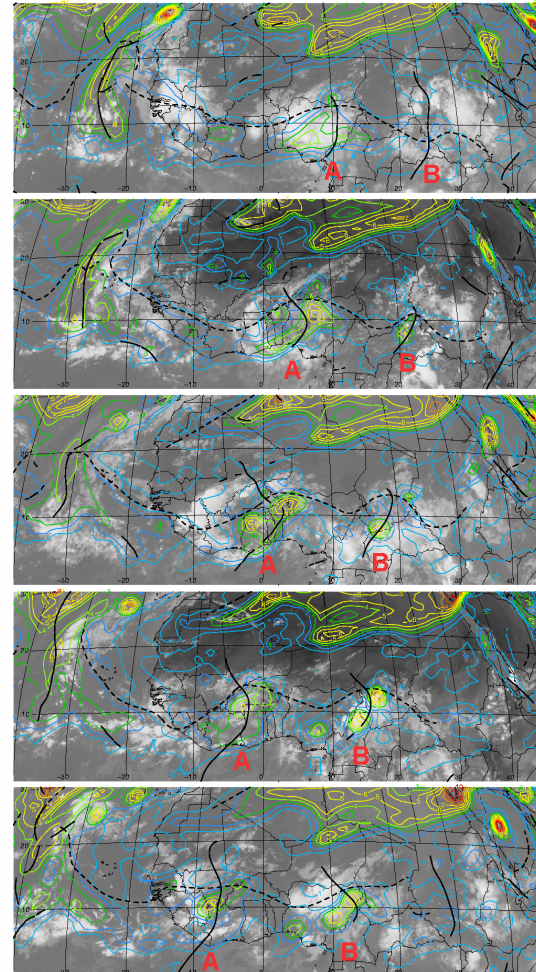


**Figure 6 –** Trough/Jet diagnostics (thick black solid and dashed contours, respectively) and 315K Potential Vorticity from GFS analyses (contoured in color, blue to red in increments of 0.1 PVU) overlaid on METEOSAT infrared imagery. Images are shown every 12 hours from 11<sup>th</sup> September 2004 at 00UTC (top) to 13<sup>th</sup> September 2004 at 00UTC (bottom). Note the AEWs labeled 'A' and 'B' were associated with the genesis of Hurricanes Karl and Lisa, respectively.

## 7. ACKNOWLEDGEMENT.

This research is supported by National Science Foundation grants ATM0138290 and ATM0507976.